Nanoscale

PAPER

View Article Online
View Journal | View Issue

Cite this: *Nanoscale*, 2017, **9**, 18281

Bright type-II photoluminescence from Mn-doped CdS/ZnSe/ZnS quantum dots with Mn^{2+} ions as exciton couplers†

Ruilin Xu,[a] Chen Liao,[a] Yanqing Xu,[b] Chunfeng Zhang,*[b] Min Xiao,[b] Lei Zhang,[a] Changgui Lu,[a] Yiping Cui [a] and Jiayu Zhang *[a]

Received 1st August 2017,
Accepted 28th October 2017

DOI: 10.1039/c7nr05670b

rsc.li/nanoscale

Mn^{2+} ions were introduced as exciton couplers to enhance the quantum yield (QY) of type-II photoluminescence (PL) from CdS/ZnSe/ZnS quantum dots (QDs) with slow hot-exciton cooling and low radiative rate. Transient absorption spectroscopy verifies the faster bleach recovery and faster peak red-shifting at the charge-transfer state. And the transient PL peak of the QDs changes from blue-shifting to red-shifting due to Mn^{2+} doping. The QY of type-II PL can be enhanced from ~35% to ~60% by Mn^{2+} doping. As the energy-transfer-stations of hot excitons during rapid ET (~100 ps), Mn^{2+} ions transform more excitons from hot to cold for emission. As the couplers of cold excitons during long thermal equilibrium (~100 ns), Mn^{2+} ions further decrease exciton trapping by strong bidirectional coupling. This work provides a unique way of acquiring high QY of type-II PL, and highlights the general law of PL enhancement in Mn-doped QDs.

Introduction

Owing to the spatial separation of photo-generated carriers, type-II quantum dots (QDs) with low self-absorption have potential applications in photovoltaics, lasing and solid-state lighting.[1–3] But they usually exhibit a low photoluminescence (PL) quantum yield (QY)[4] which is attributed to both the slow hot-exciton cooling[5–11] and the slow radiative recombination[4,12–15] resulting from the weak electron–hole coupling due to charge transfer (CT). First, hot excitons are more easily captured by traps[16] during their slow cooling. Due to the "phonon bottleneck" in QDs,[5,17,18] a hot electron can cool by transferring its energy to the hole with higher state density that then relaxes *via* phonons.[5] For type-II QDs with the electron strongly confined in cores, hot electron cooling can be markedly slowed down with the increasing shell extracting the hole to a remote state; even for the CdSe/ZnS/ZnSe/CdSe QDs with a weak type-II alignment, the slow time constant of intraband relaxation increases from ~10 ps to ~1.7 ns with ZnSe-shell thickness increasing from 0 to ~3.5 nm.[5] Second, the slow radiative recombination is a disadvantage when competed with exciton trapping.[4,19]

Recently, Mn-doped QDs with tunable dual emission was a hot topic because of QDs' potential application in nanoscale temperature sensors.[20–25] In these systems, thermal equilibrium is achieved in the limit of rapid population exchange between excitons and Mn^{2+} $^4T_1$ by the bidirectional energy transfer (ET) between them.[20–25] Due to the internal strong exciton–Mn^{2+} coupling, the ratio of excitons to Mn^{2+} emission intensities is independent of nonradiative effects.[21,22] Notably, previous related studies mainly focused on the internal competition between two transitions, while our work firstly focuses on the fact that the strong exciton–Mn^{2+} coupling can be used to enhance CT exciton emission by decreasing exciton trapping. Such an idea of enhancing exciton emission by exciton–Mn^{2+} coupling is actually implied by the photo- and thermal stability of dual-emitting QDs[20–24,26] than undoped QDs.[27–29] Especially, for the dual-emitting QDs with the small energy difference (ΔE) between exciton and excited dopant ions, they showed the intriguing total emission containing an intriguing exciton emission at high temperatures, which probably resulted from the fact that the nonradiative trapping was decreased by the strong bidirectional coupling (due to the small ΔE) at high temperatures; but the corresponding undoped QDs showed a complete thermal quenching of their emission at high temperatures.[26]

Due to the competition between Mn^{2+} ions and traps, exciton trapping is decreased, leading to a higher total PLQY

[a]*Advanced Photonic Center, Southeast University, Nanjing 210096, China. E-mail: jyzhang@seu.edu.cn*
[b]*National Laboratory of Solid State Microstructures, School of Physics, Nanjing University, Nanjing 210093, China. E-mail: cfzhang@nju.edu.cn*

†Electronic supplementary information (ESI) available. See DOI: 10.1039/c7nr05670b

than that of corresponding undoped QDs.[30–33] Specially, in such strongly coupled systems, Mn^{2+} ions possess an extremely low radiative rate due to the spin-forbidden,[30,31] leading to the fact that excitons could emit with near-unity probability despite their being ~100 meV above the Mn^{2+} $^4T_1$ state.[20] In other words, the enhanced emission by the competition between Mn^{2+} ions and traps can be mainly distributed to excitons by internal competitions of several processes.[20–25] Additionally, unlike type-I QDs, type-II QDs possess a fairly slow cooling of hot excitons, partly accounting for their low PLQY. By Mn^{2+} doping, the energy of hot excitons is rapidly transferred (~100 ps) to Mn^{2+} ions, accompanied with a faster redshifting in transient absorption (TA) spectra, which decreases the trapping of hot excitons. Based on these mechanisms, Mn^{2+} ions with a higher QY of radiative recombination were probably introduced to improve the PLQY of type-II QDs with fairly pure exciton emission.

Additionally, a thick shell of type-II QDs can enhance the PL and the photostability, besides diminishing nonradiative Auger recombination.[34–36] But the PL enhancement is limited by the decreased radiative rate,[4,37,38] in spite of introducing further ZnS capping. Accordingly, Mn^{2+} ions, as exciton couplers, were introduced to improve the QY of type-II PL (from ~35% to ~60%) of CdS/ZnSe/ZnS QDs with a thick ZnSe shell of ~10 monolayers (MLs) (~3 nm) with small oscillator strength. By the way, for core/shell1/shell2 CdS/ZnSe/ZnS (or ZnSe/CdS/ZnS) QDs, there were only a few reports on high QYs of type-II PL (≥60%).[19,38,39] Most interesting was one fact that the enhancement in brightness was due to an increase in the radiative rate[19] and was from the thin-shell1 QDs, corresponding to the quasi type-II (or type-$I^{1/2}$) regime.[13,36] This study reveals an interesting and effective effect of Mn^{2+} ions on the enhancement of type-II PL, and provides a good opportunity of summarizing the general law of PL enhancement in Mn-doped QDs.

Experimental

Chemicals

Cadmium oxide (CdO, 99.99%), zinc stearate ($ZnSt_2$, 12.5%–14% ZnO), selenium powder (Se, 99.999%), 1-octadecene (ODE, 90%), stearic acid (SA, 99%), and tri-*n*-octylphosphine oxide (TOPO, 98%) were purchased from Alfa Aesar. Manganese(II) stearate ($MnSt_2$, ≥95%) was purchased from Wako. Zinc oxide (ZnO, 99.9%), oleic acid (OA, 90%), oleylamine (OAm, 70%), sulfur (S, 99.98%), 1-dodecanethiol (DDT, ≥98%) and tri-*n*-octylphosphine (TOP, 97%) were purchased from Sigma-Aldrich. All chemicals were used directly without any further purification.

Synthesis of undoped and Mn-doped CdS QDs as seeds

To obtain high-quality QDs with monodisperse and good crystallinity, both undoped and Mn-doped CdS quantum dots were synthesized by a hot-injection strategy.[40,41] Mn-doped CdS QDs were prepared by the effective nucleation-doping strategy, following the method of Yang *et al.*[42] For QD growth by using a designed structure of MnS/ZnS/CdS ($N_{Zn} \approx 2N_{Mn} \approx 0.1N_{Cd}$; also called CdS : Mn QDs), a thin ZnS interlayer (~1 ML) was introduced to reduce the lattice mismatch between MnS and CdS, just avoiding the introduction of additional strain in Mn-doped QDs prepared by nucleation doping.[42] The PLQY of these Mn-doped QDs, prepared by us, can be as high as ~65%. Besides surface ligands, the high PLQY of these Mn-doped cores depends on good Mn^{2+} diffusion, which needs a precise control. The high PLQY of Mn-doped QDs shows no obvious sensitivity to the PLQY of these Mn-doped seed cores, because optimized "flash" synthesis at high temperature (320 °C) matches well with nucleation doping, improving the crystallinity[43–45] and further favoring the diffusion of the Mn^{2+} ions.[44,45] Undoped CdS QDs with similar size and size distribution were prepared using a similar hot-injection strategy. Dosage of precursors and the reaction time were controlled to obtain nearly the same first exciton absorption (Abs) peak at ~450 nm. Finally after purification both undoped and Mn-doped seed cores were redispersed in small amounts of ODE for the next "flash" synthesis.

Optimized "flash" synthesis of undoped and Mn-doped CdS/ZnSe/ZnS QDs

2.5 mmol of ZnO and 12.5 mmol of OA were mixed with 4 g of TOPO in a three necked flask. The reaction mixture was heated to 100 °C while flushing with argon for one hour. The temperature was then increased to ~350 °C.[44,45] After the solution became colorless, the temperature was set to 320 °C. At ~320 °C, a solution containing 80 nmol of seed QDs was injected, which was followed by a sudden temperature drop (to ~280 °C). Unlike the typical "flash" synthesis,[43] the single rapid injection of the precursor solution was changed to multiple slow injections; usually, the optimized "flash" synthesis can lead to narrower size distribution, higher QY, and breakthrough of the size limitation.[45] At 300 °C, 0.5 mmol (for ~10 ML ZnSe shells) of TOP-Se in ODE was slowly dropped in ~2 min, followed by annealing for ~5 min. And then the temperature was increased to 320 °C, followed by annealing for ~5 min. At 320 °C, the S precursor solution was slowly dropped within ~2 min, followed by annealing for ~10 min. For these QDs with ZnS shells of ~10 and ~5 MLs, the amount of S was 3.25 and 2 mmol, respectively. For these QDs with ZnS shells of ~2 MLs, the amount of S was 0.75 mmol and the annealing time was 3 min. And then the reaction was stopped by natural cooling to room temperature. The QDs were washed by precipitating ~3 times with acetone and finally were redispersed in toluene or hexane.

Optical measurements

The Abs and PL spectra were measured with a Shimadzu UV3600 spectrophotometer and an Edinburgh F900 fluorescence spectrophotometer, respectively. Transmission electron microscopy (TEM) images were recorded with one Tecnai G2 Transmission Electron Microscope and another JEM-2100 transmission electron microscope. The PLQYs were measured

using a standard dye, CdS : Mn/ZnS QDs (one-pot growth doping: ~50%),[44] or CdS : Mn QDs (hot-injection nucleation doping: ~65%)[42] of known QY as the reference material. Carrier dynamics, analyzed by TP and TA spectroscopy, was acquired at low excitation density (average QD occupancy N_{eh}: ~0.1). For TP spectroscopy, the TP spectra were obtained by a streak camera (Hamamatsu C5680). The ultrafast pump pulses were from a femtosecond laser (Legend-F-1k, Coherent, 1 kHz, 100 fs). Excitation pulses at 400 nm were obtained by doubling the fundamental wavelength in a β-barium borate (BBO) crystal. For TA spectroscopy, the carrier dynamics was probed by a broadband supercontinuum light source, generated by focusing a small portion of the femtosecond laser beam onto a sapphire plate. The chirp of the probe supercontinuum was corrected with error to be less than 100 fs over the whole spectral range. The TA signal was then analyzed by a fast charge-coupled device (S11071-1104, Hamamatsu) with a monochromator (Acton 2358, Princeton Instruments). The composition of the samples was measured by means of inductively coupled plasma optical emission spectroscopy (ICP-OES, Optima 5300 DV, PerkinElmer).

Results and discussion

Fig. 1 shows similar evolutions of Abs spectra, PL spectra and TEM images in the synthesis of undoped (Fig. 1(a–d)) and Mn-doped (Fig. 1(e–h)) CdS/ZnSe/ZnS QDs. The undoped and Mn-doped CdS seed QDs exhibit a sharp PL peak at 463 nm (band-edge emission) and a wide PL peak at ~580 nm (Mn^{2+} emission), respectively, but they show almost the same first exciton Abs peak at ~450 nm. During ZnSe shell coating, both undoped and Mn-doped CdS/ZnSe QDs exhibit obvious redshifts in the Abs edge and PL peak, which is attributed to type-II confinement of the CdS/ZnSe system (see the ESI, Fig. S1†).[14,36] During ZnS shell coating, both undoped and Mn-doped CdS/ZnSe/ZnS QDs exhibit obvious blueshifts in the PL peak, which may originate from the compressive lattice strain.[46] The optimized "flash" synthesis favors the easy acquisition of high-quality QDs with high crystallinity[43–45] and narrow size distribution;[45] and under precise control, undoped QDs and their corresponding Mn-doped QDs possess close sizes, shown by the TEM images in Fig. 1.

The full width at half maximum (FWHM) of the PL spectrum of Mn-doped CdS/ZnSe/ZnS QDs (ZnS shell: ~2 MLs; FWHM: 38 nm), is not only smaller than the FWHM of the Mn^{2+} emission spectrum (~70 nm), but also smaller than that of the corresponding undoped QDs (44 nm). Combined with the next analysis of PL decays (~100 ns), the PL from these Mn-doped CdS/ZnSe/ZnS type-II/type-I (regarded as type-II in a broad sense) QDs is mainly attributed to type-II emission. Although there is nearly no Mn^{2+} emission, there is no doubt that Mn^{2+} ions were effectively doped into the CdS/ZnSe/ZnS QDs because of several strong proofs, for example: (1) the seed cores are effectively inner-doped (see the ESI, Fig. S2†) with certain Mn^{2+} concentration (see the ESI, Table S1†); and (2) there are strong contrasts in both transient Abs and PL spectra between Mn-doped and undoped QDs. Additionally, for the Mn-doped CdS/ZnS type-I QDs with the same Mn-doped seed cores and the similar shell growth, the PL from them is mainly attributed to Mn^{2+} emission (see the ESI, Fig. S3†). That is because in Mn-doped QDs the energy difference between excitons and Mn^{2+} $^4T_1$ (ΔE) acts as the thermodynamic driving force for net ET.[25] A small ΔE will lead to a strong bidirectional exciton–Mn^{2+} $^4T_1$ coupling but nearly no Mn^{2+} emission due to the spin-forbidden. Importantly, the type-II PL is redshifted and significantly enhanced by Mn^{2+} doping, suggesting a strong exciton–Mn^{2+} coupling.

The transient PL (TP) spectra of undoped and Mn-doped CdS/ZnSe/ZnS QDs (ZnS shell: ~2 MLs) were measured by a streak camera under the same conditions. Fig. 2(a and b) exhibit a distinct contrast between these undoped and Mn-doped QDs. Compared to the undoped QDs possessing the wider and shorter TP spectrum with a blueshifting PL peak,

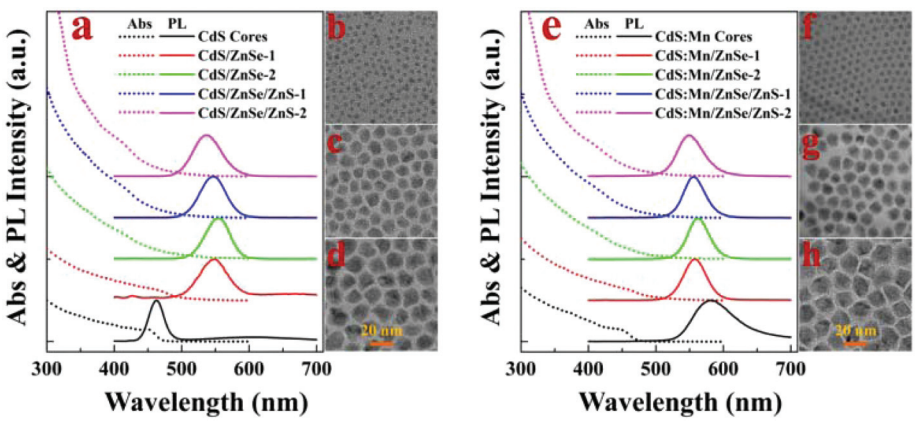

Fig. 1 Evolutions of Abs spectra, PL spectra and TEM images in the synthesis of undoped (a–d) and Mn-doped (e–h) CdS/ZnSe/ZnS QDs, respectively. Both undoped and Mn-doped CdS cores (b and f) possess a diameter of ~4 nm. ZnSe-2 denotes the QDs with a ZnSe shell of ~10 MLs (diameter: ~10.5 nm, c and g), while ZnS-1 and ZnS-2 denote the QDs with a ZnS shell of ~2 MLs and ~5 MLs (diameter: ~14 nm, d and h), respectively.

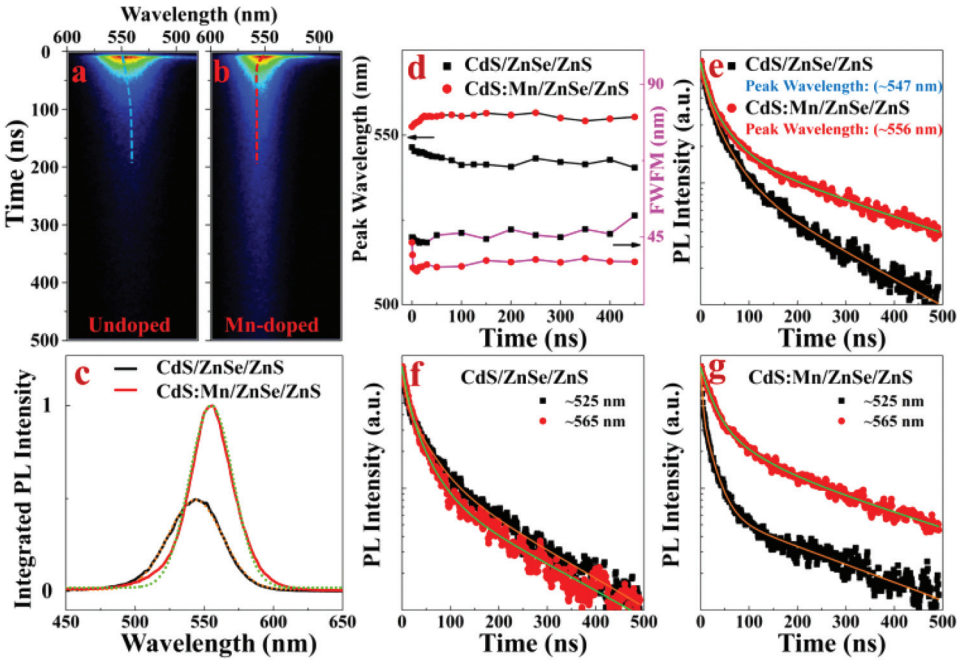

Fig. 2 (a–b) Streak camera images of time-resolved PL spectra of undoped and Mn-doped CdS/ZnSe/ZnS QDs, respectively. (c) Normalized integrated transient PL spectra of the undoped and Mn-doped QDs. (d) Evolution of the peak wavelength of the undoped and Mn-doped QDs. (e) Time resolved PL decay spectra of the undoped and Mn-doped QDs monitored at the peak wavelength. (f–g) Time resolved PL decay spectra of the undoped (f) and Mn-doped (g) QDs monitored at ~525 nm and ~565 nm, respectively.

the Mn-doped QDs possess the narrower and longer TP spectrum with a redshifting PL peak. Additionally, for the undoped QDs, a small amount of additional rapidly decaying high-energy emission (~500 nm) is attributed to an upper bright state showing even at low pump intensities, which was firstly demonstrated as an intrinsic feature of the QDs by I. Moreels and R. F. Mahrt in 2011.[47,48] In 2016 H. M. Zhu and X.-Y. Zhu further related it to hot fluorescence emission.[11] For the Mn-doped QDs, a wider more rapidly decaying high-energy emission (530–480 nm) leads to additional sharp contrast in spectrum, originating from the rapid ET from higher energy excitons to Mn^{2+} ions.

As shown in Fig. 2c, the integrated TP spectra, similar to stable PL spectra (see the ESI, Fig. S4†), show the peak redshifting, linewidth narrowing and PL enhancement (PLQY: from 37% to 63%) due to Mn^{2+} doping. Both undoped and Mn-doped QDs have the PL peak at ~550 nm at the beginning, but afterwards these undoped and Mn-doped QDs exhibit a blueshifting and a redshifting in the PL peak, respectively, shown in Fig. 2d. The PL lifetime of Mn-doped QDs (244 ns) is longer than that of undoped QDs (119 ns), shown in Fig. 2e (see the ESI,† multi-exponential fitting parameters listed in Table S1†), but they are both in the timescale of ~100 ns. Accordingly, the PL from Mn-doped QDs cannot be assigned to Mn^{2+} emission ($^4T_1$ to $^6A_1$) with the intrinsic PL lifetime in the timescale of milliseconds (ms),[49,50] but instead it should be assigned to type-II PL.[4,14,15] According to the detailed analysis (see the ESI, Table S1†), the radiative rate[51] of the Mn-doped QDs is just slightly changed owing to a rapid population exchange between excitons and Mn^{2+} $^4T_1$,[21–25] which is achieved by a strong exciton–Mn^{2+} coupling. Thus, the increased PL lifetime is mainly attributed to the decreased nonradiative rate, which is also achieved by the strong coupling.

Additionally, for the undoped QDs, the PL decay monitored at ~525 nm is slightly slower than that monitored at ~565 nm, which may originate from the intrinsic feature of type-II QDs that CT excitons with better spatial separations, reducing the exciton binding energy,[52] possessed higher energy and longer PL lifetime. While for the Mn-doped QDs, the PL decay monitored at ~525 nm is much faster than that monitored at ~565 nm, which implies that Mn^{2+} ions tend to capture higher energy excitons but feed energy back to lower energy exciton states, leading to the change in a transient PL peak from blueshifting to redshifting. Briefly, the abovementioned sharp contrast suggests a strong exciton–Mn^{2+} coupling.

TA spectra were acquired using 350 nm excitation of both undoped and Mn-doped CdS/ZnSe/ZnS samples (ZnS shell: ~5 MLs for the stability; PLQY: 26% and 50%, respectively) in methylbenzene. As shown in Fig. 3(a–d), two clearly separated bleach signals have been detected. These signals are assigned to a CT state, $1S_e$(CdS)–$1S_h$(ZnSe) ($1S_{CdS-ZnSe}$), and a localized, CdS-based exciton, $1S_e$(CdS)–$1S_h$(CdS) ($1S_{CdS}$), respectively.[9,39] Both undoped and Mn-doped QDs possess nearly the same time of bleaching growth ($1S_{CdS}$: ~1.7 ps; $1S_{CdS-ZnSe}$: ~3.6 ps) (see the ESI, Fig. S5†) and the close contour plots of TA spectra at an early stage (see the ESI, Fig. S6†), showing the similarity between the two samples. But they show a sharp contrast in

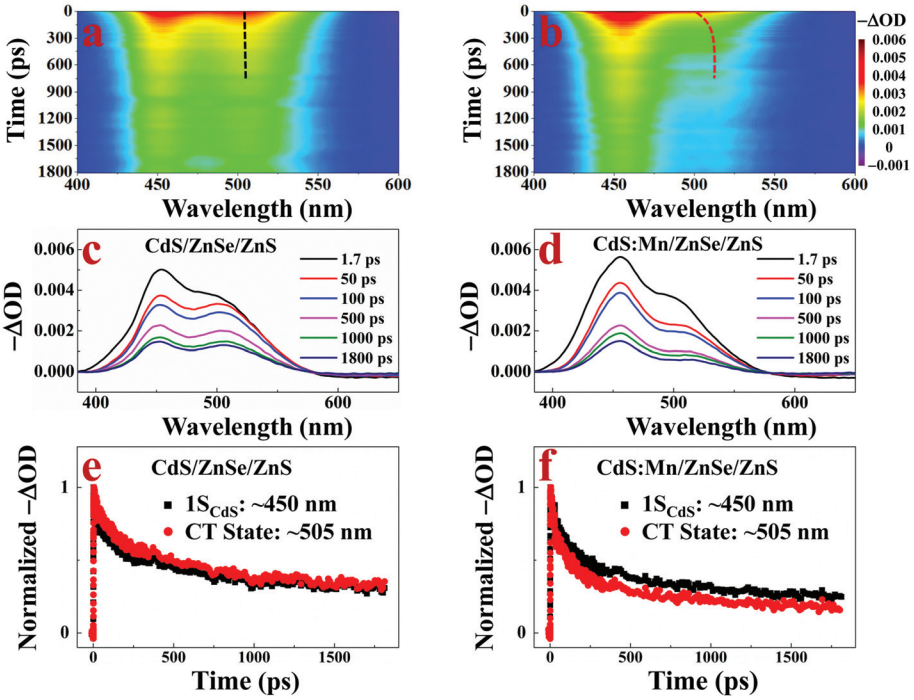

Fig. 3 (a–b) Contour plots of the experimental TA spectra of undoped (a) and Mn-doped (b) CdS/ZnSe/ZnS QDs (λ_{pump} = 350 nm). (c–d) Evolution of the TA spectra of the undoped (c) and Mn-doped (d) QDs. (e–f) TA dynamics of the undoped (e) and Mn-doped (f) QDs monitored at $1S_{CdS}$ (~450 nm) and $1S_{CdS-ZnSe}$ (*i.e.* CT state: ~505 nm), respectively.

contour plots of TA spectra within 1800 ps because of Mn^{2+} doping. For these undoped QDs, the bleach recovery probed at $1S_{CdS}$ is only faster than that probed at the CT state at an early stage, but later they are similar, shown in Fig. 3e. While for these Mn-doped QDs, bleach recovery probed at the CT state is faster than that probed at $1S_{CdS}$, shown in Fig. 3f, which indicates that there must be a rapid ET mainly from CT excitons to Mn^{2+} ions that increases the bleach recovery rate at the CT state.

Fig. 4a shows the TA dynamics of bleach recovery of undoped and Mn-doped CdS/ZnSe/ZnS QDs at a type-II Abs peak (~505 nm). The TA decay curves are fitted by multi-exponential functions, and the fitting parameters are listed in Table S2 (see the ESI†). Decay curves of undoped and Mn-doped QDs show a distinct contrast at an early stage (≤300 ps), which can be used for calculation of the ET time. The fast components are calculated by $\tau_{fast} = (A_1\tau_1 + A_2\tau_2)/(A_1 + A_2)$.[30] They are 168 ps and 96 ps carrying about 50% and 70% of the amplitude for undoped and Mn-doped QDs, respectively. Accordingly, the ET time τ_{ET} is calculated as 224 ps by[30,32]

$$1/\tau_{ET} = (1/\tau_{fast})_{doped} - (1/\tau_{fast})_{undoped}.$$

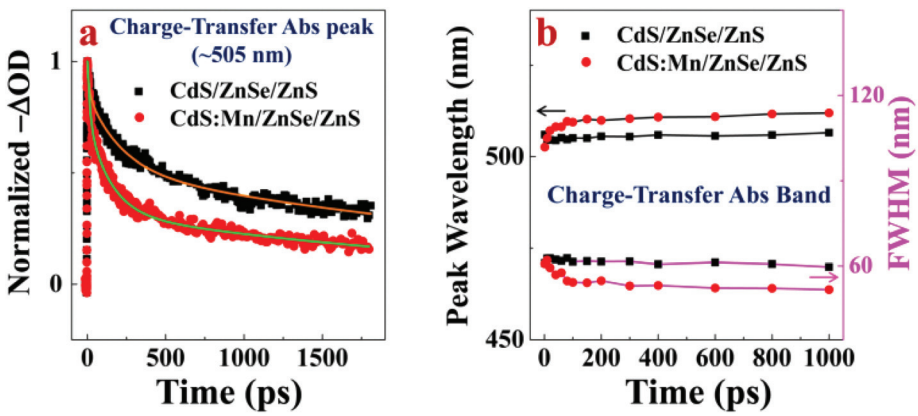

Fig. 4 (a) TA dynamics of undoped and Mn-doped CdS/ZnSe/ZnS QDs monitored at the CT Abs peak (~505 nm) and (b) evolutions in the peak wavelength and FWHM of TA spectra of the CT state.

Fig. 4b shows evolutions of the peak wavelength and the FWHM of the TA spectra of the CT state. For the undoped QDs, there are no obvious changes in both of them. Usually, the TA peak gradually redshifts toward longer wavelengths.[9] The fairly slow redshift suggests that the high-energy carriers decay to the bottom of the band very slowly,[9] resulting from the weak electron–hole coupling.[5,8,9] Such slow cooling of hot excitons is against the high QY of type-II PL, whereas for the Mn-doped QDs, the peak of the TA spectra of the CT state is redshifted obviously, and the FWHM of the TA spectra of the CT state is decreased significantly, which are also vividly depicted in Fig. 3 (a and b). Both changes mainly occur within 300 ps, consistent with the ET time (~220 ps), which suggests that the faster cooling of hot excitons is attributed to the ET from hotter excitons to Mn^{2+} ions, favoring a higher QY of type-II PL.

For TA spectra monitored at ~505 nm, Mn-doped CdS/ZnSe/ZnS QDs exhibit faster bleach recovery and faster peak red-shifting at the CT state than those the corresponding undoped QDs exhibit. While for TP spectra monitored at ~550 nm, these Mn-doped QDs exhibit slower PL decay than that the corresponding undoped QDs exhibit. The slower PL decay is partly attributed to the back feeding to the lower energy exciton states. The back energy transfer does not show in the TA spectra (~2 ns) obviously because the back ET is in the longer timescale of ≥10 ns. A back ET in the timescale of ~1 μs was reported in the Mn-doped QDs (PL peak: ~520 nm) with larger energy difference between excitons and Mn^{2+} $^4T_1$ (ΔE).[20] The back ET in these Mn-doped CdS/ZnSe/ZnS QDs (bright type-II PL peak: ~550 nm) is in the timescale of ~10–100 ns corresponding to a certain range of ΔE values. In conclusion, for these Mn-doped QDs, there is a strong contrast between the faster decay in the TA spectra (~505 nm) and the slower decay in the TP spectra (~550 nm), which reveal the rapid ET to Mn^{2+} ions (~100 ps) and the slow back ET to exciton states (~10–100 ns), respectively.

Fig. 5 shows the schematic diagram of energy evolution in Mn-doped type-II QDs. The "strongly coupled" scenario shows two exciton–Mn^{2+} couplings: the rapid ET from hot CT excitons to Mn^{2+} ions as coupling-1 and the strong bidirectional coupling between cold ("relaxed") CT excitons and Mn^{2+} $^4T_1$ as coupling-2, *i.e.* forward (k_{ET}) and thermally assisted back (k_{BET}) ET between the host and Mn^{2+} ions.[20–25] The strong coupling-2 leads to a rapid population exchange between two emissive states, *i.e.* cold excitons and Mn^{2+} $^4T_1$, which establishes the thermal equilibrium of these two excited states.[22] With the increasing population of Mn^{2+} $^4T_1$ (N_{Mn^*}) and the increasing k_{BET} (back coupling to colder exciton states), the bidirectional coupling reaches the strongest value at thermal equilibrium ($k_{ET}N_{exc} \approx k_{BET}N_{Mn^*}$). Usually type-II QDs possess a large Stokes-shift and slow hot-exciton cooling. Accordingly, in Mn-doped type-II QDs the slow intrinsic cooling of hot CT excitons provides a chance that the energy of some hot CT excitons transfers to Mn^{2+} ions, followed by the establishment of thermal equilibrium between cold excitons and Mn^{2+} $^4T_1$. This scenario is different from the "strongly coupled" scenario in Mn-doped type-I QDs with fast hot-exciton cooling that the thermal equilibrium between excitons and Mn^{2+} $^4T_1$ can establish mainly after the hot-exciton cooling. Further, our work focuses on the fact that strong exciton–Mn^{2+} coupling can be used to enhance CT exciton emission by decreasing the trapping of both hot and cold excitons. Additionally, the ET from CT excitons to Mn^{2+} ions (~100 ps) is orders of magnitude faster than the slower radiative decays of CT excitons (~100 ns) and Mn^{2+} $^4T_1$ (~1 ms); accordingly, these two excited states of CT excitons and Mn^{2+} $^4T_1$ are strongly coupled.[22] As shown in the inset of Fig. 5, Mn-doped CdS/ZnSe/ZnS QDs exhibit a distinctly brighter and redshifted PL than the corresponding undoped QDs, verifying a strong exciton–Mn^{2+} coupling.

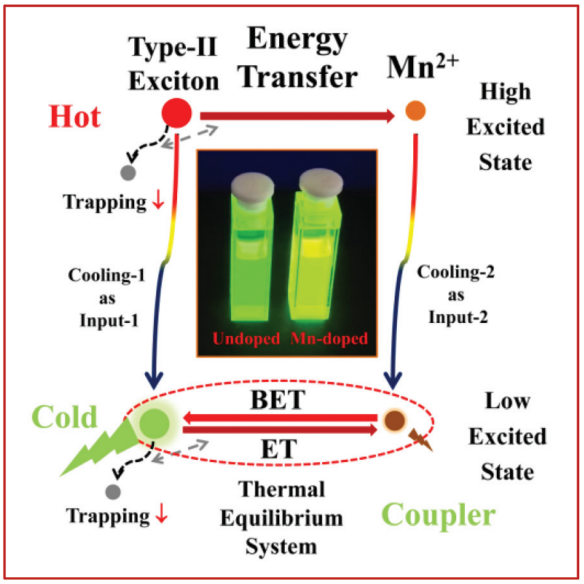

Fig. 5 Schematic diagram of energy evolution in Mn-doped QDs with the slow intrinsic cooling of hot CT excitons; inset: undoped and Mn-doped CdS/ZnSe/ZnS QDs in *n*-hexane under a UV lamp.

Due to the strong coupling, exciton trapping is decreased, resulting in a higher PLQY than the undoped QDs.[26,30] The enhancement of PLQY is attributed to the whole system of excitons and Mn^{2+} $^4T_1$. But in the system, the enhanced emission will be distributed to excitons and Mn^{2+} $^4T_1$ according to the internal ratio of two PL intensities; and they can be mainly distributed to excitons (≥95%) at room temperature, despite their being ~100 meV above Mn^{2+} $^4T_1$ with extremely low radiative rate due to the spin-forbidden.[20] The thermal equilibrium in Mn-doped type-I QDs has been systematically studied, while there is still a divergence on the population statistics of the strongly coupled excited states. A parameter of α ($\alpha < 1$) was introduced into the Boltzmann equation by W. Y. Liu and V. I. Klimov to agree with the experiments,[25] and then the relationship between populations of excitons (N_{exc}) and Mn^{2+} $^4T_1$ (N_{Mn^*}) can be expressed as

$$N_{exc} = N_{Mn^*}e^{-\alpha\Delta E/kT};$$

"$\alpha < 1$" means that the decrease in the population of higher energy excited states in a coupled system is suppressed when

compared with the decrease governed by classical Boltzmann statistics. In the article with the introduction of "α", a rigorous physical interpretation of α is not yet available, and it was assigned as a materials-specific constant. Probably, a Schrodinger cat lives in the strongly coupled system, which leads to the divergence and unclarity. Factually, the "strongly coupled" system with rapid population exchange should be governed by the superposition principle of quantum mechanics, and the strong coupling probably suppresses the decrease in the population of higher energy states, which can be depicted by "α". Importantly, this hypothesis also agrees with the literature from D. R. Gamelin's group, where Mn^{2+} $^4T_1$ coupled to the exciton states with higher energy in experiments than that in stimulation by classical Boltzmann statistics.[20,21] To conclude, the strong bidirectional coupling favors the nearly unchanged radiative rate (see the ESI, Fig. S7†) and the fairly pure exciton emission.

In detail, from the formation of hot CT excitons to the established thermal equilibrium between cold CT excitons and Mn^{2+} $^4T_1$, there are two competing paths for transferring the energy into the thermal-equilibrium-system, shown in Fig. 5: one is the direct slow cooling of hot excitons, and the other is the rapid ET from hot excitons to Mn^{2+} ions by the coupling between hot excitons and high excited states of Mn^{2+}, followed by the cooling of excited Mn^{2+} ions. Usually, hot excitons were more easily captured by traps during their slow cooling.[16] The latter path is an effective one for transferring more energy into the system due to the competition between Mn^{2+} ions and traps. Slow cooling of hotter CT excitons is replaced by the latter through the rapid ET from hotter excitons to Mn^{2+} ions. Accordingly, more energy will be transferred into the thermal-equilibrium-system. Furthermore, due to the strong bidirectional coupling between excitons and Mn^{2+} $^4T_1$ in such a system, the competition between Mn^{2+} ions and traps continues to decrease the nonradiative exciton trapping. In summary, Mn^{2+} ions as exciton couplers enhance the PLQY by the strong coupling of rapid ET (coupling-1) and the strong bidirectional coupling (coupling-2). As the ETSs of hot excitons, Mn^{2+} ions transform more excitons from hot to cold for emission. As the couplers of cold excitons, Mn^{2+} ions further decrease the exciton trapping by coupling-2. The PLQY is enhanced by the continuous competition between Mn^{2+} ions and traps in both processes of rapid ET and long thermal equilibrium. In this sense, the competition between Mn^{2+} ions and traps during thermal equilibrium with strong exciton-Mn^{2+} $^4T_1$ coupling is similar to that during rapid ET from hot excitons to Mn^{2+} ions. But differently, the first competition during rapid ET is just for more potential Mn^{2+} emission by decreasing both exciton trapping and potential exciton emission. However, the second competition during the strong bidirectional coupling is mainly for more exciton emission (with slightly changed radiative rate) by decreasing exciton trapping, which means a decreased nonradiative rate. By the way, it has been reported that the nonradiative rate can also be suppressed by a strong localized-plasmon coupling.[53–55] Obviously, for an exciton, the trapping by defects will be suppressed by the strong couplings from several Mn^{2+} ions, each of which acts as a potential exciton coupler.

According to the kinetic models containing energy diagrams (see the ESI, Fig. S8†), the detailed analysis is discussed. In brief, the PL enhancement factor (PEF) due to coupling-1 (PEF1) can be estimated by the analysis of TA. The PEF due to coupling-2 (PEF2) cannot be measured separately, but can be deduced by the combination of TA and TP (or the corresponding PLQY). That is because the PL decay can also be slowed down by feeding back the energy from Mn^{2+} $^4T_1$ to exciton states (a slow shift in thermal equilibrium), besides by reducing nonradiative transition due to coupling-2. The PEF for the above-mentioned two successive processes equals the product of PEF1 and PEF2 (see the ESI, Fig. S9†). For the Mn-doped QDs with an ultra-large ΔE, the total PEF is mainly attributed to coupling-1, which means that PEF2 is approximately equal to 1. However, for the Mn-doped QDs with a small ΔE, the total PEF is mainly attributed to coupling-2, which means that PEF1 is approximately equal to 1. For the former situation, the PL lifetime is long, and Mn^{2+} ions act as energy storage; while for the latter situation, the PL lifetime is short, and Mn^{2+} ions act as exciton couplers (in a narrow sense); and for the third situation in between the previous two, Mn^{2+} ions act as exciton storage sites.[20–25] To make it more understandable, we firstly summed up the general law of PL enhancements in Mn-doped quantum dots, which is clearly shown in Fig. S10 (see the ESI†).

Usually, it is hard to prepare defect-free core/shell1/shell2 type-II/type-I QDs; so Mn^{2+} doping is an effective method to improve the QY of type-II PL. To decrease the defects, the hot-injection synthesis and optimized "flash" synthesis were used to obtain seed cores (diameter: ~4 nm) and ZnSe/ZnS shells (ZnSe shell: ~10 MLs), respectively. For the undoped CdS/ZnSe/ZnS QDs with ZnS shells of ~5 MLs and ~2 MLs, respectively, the QYs of type-II PL were ~25% and ~35%, respectively (acceptable). And then the QYs of type-II PL were easily enhanced to ~50% and ~60%, respectively, by Mn^{2+} doping. Probably, optimizations of Mn^{2+} doping will further favor a more significant increase in PLQY. Additionally, we firstly observed more significant PL enhancements (from $\leq$10% to ~35%) in similar QDs with different seed cores prepared by a one-pot strategy. For higher PLQYs, in this careful study we improved the seed cores' quality by a hot-injection strategy, accompanied with a change from growth doping to another effective nucleation doping.[42,45]

Conclusions

In conclusion, Mn^{2+} ions as exciton couplers enhance the type-II PL from CdS/ZnSe/ZnS QDs. During the rapid ET (~100 ps), Mn-doped QDs show a faster peak redshifting at the CT state, which reveals that Mn^{2+} ions promote the cooling of hot CT excitons. Furthermore, the transient PL peak of the QDs changes from blueshifting to redshifting due to exciton–Mn^{2+} coupling. As the ETSs of hot excitons, Mn^{2+} ions transform

more excitons from hot to cold for type-II emission; as the couplers of cold excitons, Mn^{2+} ions further decrease exciton trapping by strong bidirectional coupling between excitons and Mn^{2+} $^4T_1$. The enhancement of exciton emission is not due to the increase in the radiative rate, but to the suppression of the nonradiative rate by the continuous exciton–Mn^{2+} coupling. This work provides a unique way of acquiring high QY of type-II PL and highlights the general law of PL enhancement in Mn-doped QDs.

Conflicts of interest

There are no conflicts to declare.

Acknowledgements

This work was supported by the National Basic Research Program of China (973 Program, 2015CB352002), the Science and Technology Department of Jiangsu Province (BE2016021), the Fundamental Research Funds for the Central Universities (2242017 K41009) and the Postgraduate Research & Practice Innovation Program of Jiangsu Province (KYCX17_0064).

Notes and references

1 J. Bang, J. Park, J. H. Lee, N. Won, J. Nam, J. Lim, B. Y. Chang, H. J. Lee, B. Chon, J. Shin, J. B. Park, J. H. Choi, K. Cho, S. M. Park, T. Joo and S. Kim, *Chem. Mater.*, 2010, **22**, 233–240.
2 V. I. Klimov, S. A. Ivanov, J. Nanda, M. Achermann, I. Bezel, J. A. McGuire and A. Piryatinski, *Nature*, 2007, **447**, 441–446.
3 N. Kholmicheva, N. Razgoniaeva, P. Yadav, A. Lahey, C. Erickson, P. Moroz, D. Gamelin and M. Zamkov, *J. Phys. Chem. C*, 2017, **121**, 1477–1487.
4 S. S. Lo, T. Mirkovic, C.-H. Chuang, C. Burda and G. D. Scholes, *Adv. Mater.*, 2011, **23**, 180–197.
5 A. Pandey and P. Guyot-Sionnest, *Science*, 2008, **322**, 929–932.
6 C.-H. Chuang, X. Chen and C. Burda, *Ann. Phys.*, 2013, **525**, 43–48.
7 C.-H. Chuang and C. Burda, *J. Phys. Chem. Lett.*, 2012, **3**, 1921–1927.
8 C. K. Yong, J. Wong-Leung, H. J. Joyce, J. Lloyd-Hughes, Q. Gao, H. H. Tan, C. Jagadish, M. B. Johnston and L. M. Herz, *Nano Lett.*, 2013, **13**, 4280–4287.
9 N. N. Hewa-Kasakarage, M. Kirsanova, A. Nemchinov, N. Schmall, P. Z. El-Khoury, A. N. Tarnovsky and M. Zamkov, *J. Am. Chem. Soc.*, 2009, **131**, 1328–1334.
10 F. Boxberg and J. Tulkki, *Rep. Prog. Phys.*, 2007, **70**, 1425–1471.
11 H. Zhu, K. Miyata, Y. Fu, J. Wang, P. P. Joshi, D. Niesner, K. W. Williams, S. Jin and X.-Y. Zhu, *Science*, 2016, **353**, 1409–1413.
12 J. He, H. Zhong and G. D. Scholes, *Phys. Rev. Lett.*, 2010, **105**, 046601.
13 A. G. del Águila, E. Groeneveld, J. C. Maan, C. de Mello Donegá and P. C. M. Christianen, *ACS Nano*, 2016, **10**, 4102–4110.
14 S. Verma, S. Kaniyankandy and H. N. Ghosh, *J. Phys. Chem. C*, 2013, **117**, 10901–10908.
15 S. A. Ivanov and M. Achermann, *ACS Nano*, 2010, **4**, 5994–6000.
16 M. Righetto, A. Minotto and R. Bozio, *J. Phys. Chem. C*, 2017, **121**, 896–902.
17 J. Urayama, T. B. Norris, J. Singh and P. Bhattacharya, *Phys. Rev. Lett.*, 2001, **86**, 4930–4933.
18 R. Heitz, H. Born, F. Guffarth, O. Stier, A. Schliwa, A. Hoffmann and D. Bimberg, *Phys. Rev. B: Condens. Matter*, 2001, **64**, 241305.
19 C. M. Tyrakowski, A. Shamirian, C. E. Rowland, H. Shen, A. Das, R. D. Schaller and P. T. Snee, *Chem. Mater.*, 2015, **27**, 7276–7281.
20 R. Beaulac, P. I. Archer, J. van Rijssel, A. Meijerink and D. R. Gamelin, *Nano Lett.*, 2008, **8**, 2949–2953.
21 V. A. Vlaskin, N. Janssen, J. van Rjssel, R. Beaulac and D. R. Gamelin, *Nano Lett.*, 2010, **10**, 3670–3674.
22 E. J. McLaurin, L. R. Bradshaw and D. R. Gamelin, *Chem. Mater.*, 2013, **25**, 1283–1292.
23 E. J. McLaurin, V. A. Vlaskin and D. R. Gamelin, *J. Am. Chem. Soc.*, 2011, **133**, 14978–14980.
24 C.-H. Hsia, A. Wutting and H. Yang, *ACS Nano*, 2011, **5**, 9511–9522.
25 W. Liu, Q. Lin, H. Li, K. Wu, I. Robel, J. M. Pietryga and V. I. Klimov, *J. Am. Chem. Soc.*, 2016, **138**, 14954–14961.
26 Y. Liu, J. Lu and J. Zhu, *Nanoscale*, 2013, **5**, 4177–4180.
27 G. W. Walker, V. C. Sundar, C. M. Rudzinski, A. W. Wun, M. G. Bawendi and D. G. Nocera, *Appl. Phys. Lett.*, 2003, **83**, 3555–3557.
28 B. Han, W. L. Hanson, K. Bensalah, A. Tuncel, J. M. Stern and J. A. Cadeddu, *Ann. Biomed. Eng.*, 2009, **37**, 1230–1239.
29 S. Kalytchuk, O. Zhovtiuk, S. V. Kershaw, R. Zbořil and A. L. Rogach, *Small*, 2016, **12**, 466–476.
30 H.-Y. Chen, S. Maiti and D. H. Son, *ACS Nano*, 2012, **6**, 583–591.
31 C. Pu, J. Ma, H. Qin, M. Yan, T. Fu, Y. Niu, X. Yang, Y. Huang, F. Zhao and X. Peng, *ACS Cent. Sci.*, 2016, **2**, 32–39.
32 H.-Y. Chen, T.-Y. Chen and D. H. Son, *J. Phys. Chem. C*, 2010, **114**, 4418–4423.
33 S. Acharya, D. D. Sarma, N. R. Jana and N. Pradhan, *J. Phys. Chem. Lett.*, 2010, **1**, 485–488.
34 A. M. Dennis, B. D. Mangum, A. Piryatinski, Y.-S. Park, D. C. Hannah, J. L. Casson, D. J. Williams, R. D. Schaller, H. Htoon and J. A. Hollingsworth, *Nano Lett.*, 2012, **12**, 5545–5551.
35 K. P. Acharya, H. M. Nguyen, M. Paulite, A. Piryatinski, J. Zhang, J. L. Casson, H. Xu, H. Htoon and J. A. Hollingsworth, *J. Am. Chem. Soc.*, 2015, **137**, 3755–3758.

36 S. A. Ivanov, A. Piryatinski, J. Nanda, S. Tretiak, K. R. Zavadil, W. O. Wallace, D. Werder and V. I. Klimov, *J. Am. Chem. Soc.*, 2007, **129**, 11708–11719.
37 Q. Zeng, X. Kong, Y. Sun, Y. Zhang, L. Tu, J. Zhao and H. Zhang, *J. Phys. Chem. C*, 2008, **112**, 8587–8593.
38 J. Z. Niu, H. Shen, C. Zhou, W. Xu, X. Li, H. Wang, S. Lou, Z. Du and L. S. Li, *Dalton Trans.*, 2010, **39**, 3308–3314.
39 K. Boldt, K. N. Schwarz, N. Kirkwood, T. A. Smith and P. Mulvaney, *J. Phys. Chem. C*, 2014, **118**, 13276–13284.
40 W. W. Yu and X. Peng, *Angew. Chem., Int. Ed.*, 2002, **41**, 2368–2371.
41 N. Pradhan and X. Peng, *J. Am. Chem. Soc.*, 2007, **129**, 3339–3347.
42 S. Cao, J. Zheng, J. Zhao, L. Wang, F. Gao, G. Wei, R. Zeng, L. Tian and W. Yang, *J. Mater. Chem. C*, 2013, **1**, 2540–2547.
43 M. Cirillo, T. Aubert, R. Gomes, R. Van Deun, P. Emplit, A. Biermann, H. Lange, C. Thomsen, E. Brainis and Z. Hens, *Chem. Mater.*, 2014, **26**, 1154–1160.
44 R. Xu, C. Liao, H. Zhang, B. Huang, K. Fan, X. Gao, Y. Cui and J. Zhang, *RSC Adv.*, 2015, **5**, 88921–88927.
45 R. Xu, B. Huang, T. Wang, Y. Yuang, L. Zhang, C. Lu, Y. Cui and J. Zhang, *Superlattices Microstruct.*, 2017, **111**, 665–670.
46 Y.-K. Kim, S.-H. Ahn, K. Chung, Y.-S. Cho and C.-J. Choi, *J. Mater. Chem.*, 2012, **22**, 1516–1520.
47 I. Moreels, G. Rainò, R. Gomes, Z. Hens, T. Stöferle and R. F. Mahrt, *ACS Nano*, 2011, **5**, 8033–8039.
48 G. Rainò, I. Moreels, A. Hassinen, T. Stöferle, Z. Hens and R. F. Mahrt, *Nano Lett.*, 2012, **12**, 5224–5229.
49 P. Wu, J.-B. Pan, X.-L. Li, X. Hou, J.-J. Xu and H.-Y. Chen, *Chem. – Eur. J.*, 2015, **21**, 5129–5135.
50 S. Cao, C. Li, L. Wang, M. Shang, G. Wei, J. Zheng and W. Yang, *Sci. Rep.*, 2014, **4**, 7510.
51 C. Pu, H. Qin, Y. Gao, J. Zhou, P. Wang and X. Peng, *J. Am. Chem. Soc.*, 2017, **139**, 3302–3311.
52 M. H. Degani and G. A. Farias, *Phys. Rev. B: Condens. Matter*, 1990, **42**, 11701–11707.
53 L. Hu, H. Wu, C. Cai, T. Xu, B. Zhang, S. Jin, Z. Wan and X. Wei, *J. Phys. Chem. C*, 2012, **116**, 11283–11291.
54 L. Hu, H. Wu, B. Zhang, L. Du, T. Xu, Y. Chen and Y. Zhang, *Small*, 2014, **10**, 3099–3109.
55 C. Liao, L. Tang, X. Gao, R. Xu, H. Zhang, Y. Yu, C. Lu, Y. Cui and J. Zhang, *Nanoscale*, 2015, **7**, 20607–20613.